

<https://helda.helsinki.fi>

Fibroblast subsets in non-small cell lung cancer : Associations with survival, mutations, and immune features

Pellinen, Teijo

2023-01-10

Pellinen , T , Paavolainen , L , Martin-Bernabe , A , Araujo , R P , Strell , C , Mezheyeuski , A , Backman , M , La Fleur , L , Brück , O , Sjolund , J , Holmberg , E , Välimäki , K , Brunnström , H , Botling , J , Moreno-Ruiz , P , Kallioniemi , O , Micke , P & Östman , A 2023 , ' Fibroblast subsets in non-small cell lung cancer : Associations with survival, mutations, p̃y and immune features ' , Journal of the National Cancer Institute , vol. . <https://doi.org/10.1093/jnci/djac178>

<http://hdl.handle.net/10138/354042>

<https://doi.org/10.1093/jnci/djac178>

cc_by

publishedVersion





Downloaded from Helda, University of Helsinki institutional repository.

This is an electronic reprint of the original article.

This reprint may differ from the original in pagination and typographic detail.

Please cite the original version.

Fibroblast subsets in non-small cell lung cancer: Associations with survival, mutations, and immune features

Teijo Pellinen , PhD,^{1,*} Lassi Paavolainen, PhD,^{1,†} Alfonso Martín-Bernabé, PhD,^{2,†} Renata Papatella Araujo, MS,² Carina Strell , PhD,³ Artur Mezheyeuski, MD, PhD,³ Max Backman, MD, PhD,³ Linnea La Fleur, PhD,³ Oscar Brück, MD, PhD,⁴ Jonas Sjölund, PhD,⁵ Erik Holmberg , PhD,⁶ Katja Välimäki, B.Tech,¹ Hans Brunnström , MD, PhD,⁷ Johan Botling, MD, PhD,³ Pablo Moreno-Ruiz, PhD,² Olli Kallioniemi, MD, PhD,^{1,2,8} Patrick Micke, MD, PhD,^{3,†} Arne Östman, MD, PhD^{2,†}

¹Institute for Molecular Medicine Finland, Helsinki Institute of Life Science, University of Helsinki, Helsinki, Finland

²Department of Oncology-Pathology, Karolinska Institutet, Stockholm, Sweden

³Department of Immunology, Genetics and Pathology, Uppsala University, Uppsala, Sweden

⁴Hematology Research Unit Helsinki, University of Helsinki and Comprehensive Cancer Center, Helsinki University Hospital, Helsinki, Finland

⁵Division of Translational Cancer Research, Department of Laboratory Medicine, Lund University Cancer Centre, Lund University, Sweden

⁶Department of Oncology, Institute of Clinical Sciences, Sahlgrenska Academy, University of Gothenburg, Sahlgrenska University Hospital, Gothenburg, Sweden

⁷Division of Pathology, Lund University, Skåne University Hospital, Lund, Sweden

⁸Science for Life Laboratory (SciLifeLab), Department of Oncology-Pathology, Karolinska Institutet, Stockholm, Sweden

[†]Authors contributed equally to this work.

*Correspondence to: Teijo Pellinen, PhD, Institute for Molecular Medicine Finland (FIMM), Helsinki Institute of Life Science, University of Helsinki, Tukholmankatu 8, 00290, Helsinki, Finland (e-mail: teijo.pellinen@helsinki.fi).

Abstract

Background: Cancer-associated fibroblasts (CAFs) are molecularly heterogeneous mesenchymal cells that interact with malignant cells and immune cells and confer anti- and protumorigenic functions. Prior in situ profiling studies of human CAFs have largely relied on scoring single markers, thus presenting a limited view of their molecular complexity. Our objective was to study the complex spatial tumor microenvironment of non-small cell lung cancer (NSCLC) with multiple CAF biomarkers, identify novel CAF subsets, and explore their associations with patient outcome.

Methods: Multiplex fluorescence immunohistochemistry was employed to spatially profile the CAF landscape in 2 population-based NSCLC cohorts (n = 636) using antibodies against 4 fibroblast markers: platelet-derived growth factor receptor-alpha (PDGFRA) and -beta (PDGFRB), fibroblast activation protein (FAP), and alpha-smooth muscle actin (α SMA). The CAF subsets were analyzed for their correlations with mutations, immune characteristics, and clinical variables as well as overall survival.

Results: Two CAF subsets, CAF7 (PDGFRA-/PDGFRB+/FAP+/ α SMA+) and CAF13 (PDGFRA+/PDGFRB+/FAP-/ α SMA+), showed statistically significant but opposite associations with tumor histology, driver mutations (tumor protein p53 [TP53] and epidermal growth factor receptor [EGFR]), immune features (programmed death-ligand 1 and CD163), and prognosis. In patients with early stage tumors (pathological tumor-node-metastasis IA-IB), CAF7 and CAF13 acted as independent prognostic factors.

Conclusions: Multimarker-defined CAF subsets were identified through high-content spatial profiling. The robust associations of CAFs with driver mutations, immune features, and outcome suggest CAFs as essential factors in NSCLC progression and warrant further studies to explore their potential as biomarkers or therapeutic targets. This study also highlights multiplex fluorescence immunohistochemistry-based CAF profiling as a powerful tool for the discovery of clinically relevant CAF subsets.

Cancer-associated fibroblasts (CAFs) are constituents of common solid tumors [reviewed in (1-3)]. CAFs interact with other cell types in the tumor microenvironment, including malignant cells, immune cells, and cells of the vasculature. Experimental studies imply CAFs as regulators of proliferation, migration, epithelial-mesenchymal transition, and stem-cell properties of malignant cells. Immunoregulatory mechanisms have been suggested, such as recruitment of myeloid-derived suppressor cells, negative effects on CD8+ cell proliferation and activity, and support of regulatory CD4+ cells [reviewed in (4,5)]. Notably, studies outside of tumor biology have identified instructive functions of fibroblasts affecting epithelial cells and immune cells [reviewed in (6,7)].

Recent studies have indicated the existence of clinically relevant subsets of fibroblasts with differential functional activities. Most studies in the field have employed single-cell RNA sequencing approaches or multimarker fluorescence-activated cell sorting (8-13). Considerable interpatient variability and association with prognosis and treatment response have been detected (8-13). These studies have, with few exceptions, relied on single-marker staining with reduced resolution. The mechanisms shaping interpatient variability in CAF composition remain unknown. However, studies in mouse models suggest a role of driver mutations in malignant cells (14).

Commonly used fibroblast markers include platelet-derived growth factor receptor alpha (PDGFRA) and beta (PDGFRB),

Received: March 08, 2022. Revised: June 30, 2022. Accepted: September 06, 2022

© The Author(s) 2022. Published by Oxford University Press.

This is an Open Access article distributed under the terms of the Creative Commons Attribution License (<https://creativecommons.org/licenses/by/4.0/>), which permits unrestricted reuse, distribution, and reproduction in any medium, provided the original work is properly cited.

fibroblast activation protein (FAP), and alpha-smooth muscle actin (α SMA). The PDGF and PDGFR axis is one of the hallmark pathways controlling growth and migration of fibroblasts in tissue repair and development (15). FAP is a well-studied marker of fibroblasts in tissue fibrosis, often also upregulated in CAFs, and has lately been subjected to various targeting approaches (16). Finally, α SMA has long been used as a marker for activated fibroblasts with contractile features [reviewed in (1-3)]. With few exceptions (17), earlier studies mostly report results from analyses of single markers. It thus remains largely unknown how CAF markers are co-expressed.

Model studies suggest important roles of CAFs in non-small cell lung cancer (NSCLC) (18-21). Furthermore, immunohistochemical studies with single markers have indicated partly inconsistent prognosis associations of single marker-defined CAF subsets (22-25). Recent single-cell RNA sequencing studies of digested lung cancer tissue have suggested high CAF heterogeneity (26,27).

The aim of this study was to apply multiplex immunofluorescence staining and a deep learning-based image analysis pipeline to well-annotated NSCLC cohorts to quantitate multimarker-defined CAF subsets and characterize their clinical relevance.

Methods

Patient material, tumor data, and tissue microarrays (TMAs)

The patient population and associated TMAs have been described earlier [see (28-31) and [Supplementary Methods](#), available online]. In brief, each TMA included more than 350 patient cases from 2 population-based NSCLC collections (BOMI1 and BOMI2). Multiplex tissue staining with high quality tissue was performed on 318 patient cases from both cohorts, respectively (see flow diagram of included patients, [Supplementary Figure 1](#), available online).

Multiplex fluorescent immunohistochemical staining and image capturing

Multiple fluorescent immunohistochemical staining and imaging were performed in 2 cycles ([Supplementary Table 1](#), available online). After the first-round staining and whole-slide imaging of the TMAs, the fluorescence signal was bleached, and the antibodies from the first-round staining were denatured, after which the second-round staining was performed as shown in [Supplementary Table 1](#) (available online).

Imaging of the BOMI2 cohort was performed by a Metafer5 scanning and imaging platform (MetaSystems, Germany; detailed specs shown in the [Supplementary Methods](#), available online). Images were exported as 1 image per TMA spot formatted as lossless-compressed single-channel 8-bit tag image file format images. Images were exported as 100% and 25% resolution for cell segmentation as well as for epithelial and stromal segmentation, respectively. Imaging for BOMI1 was performed using a Zeiss Axio Scan.Z1 with specs described in the [Supplementary Methods](#) (available online). Images were exported as whole-slide 16-bit tag image file format single-channel greyscale images (25% and 100% resolution images).

Image processing and analyses

For a complete description of TMA spot image cropping, image registration, epithelium and autofluorescence masks, cell segmentation, and intensity measurement, see the [Supplementary Methods](#) (available online). TMA spots were identified (32), and

the first- and second-round TMA spot images were aligned based on nuclear 4',6-diamidino-2-phenylindole signal. Pixel classification module of ilastik (33) was used to detect the epithelium/stroma and red blood cells (autofluorescence) (34). Nuclei segmentation details are shown in the [Supplementary Methods](#) (available online). Briefly, nuclei were segmented from 4',6-diamidino-2-phenylindole channel with a pretrained deep learning segmentation model (35), and cell regions were defined by dilating the nuclear segmentation. Mean channel intensity of individual markers colocalizing in each segmented cell was determined. Distance of each cell to the epithelial mask was also determined.

Cell classification to 15 different CAF subsets

For full description, see [Supplementary Methods](#) (available online). Based on histograms and visual confirmation, we used the mean intensity + 1.0*stdev (standard deviation) in tumor cells to define the positivity thresholds of each stromal marker in stromal cells except for using mean + 2.0*stdev for PDGFRB in the BOMI1 cohort, where the signal was stronger than in the BOMI2 cohort. Based on status of the 4 markers, cells were classified into 15 subgroups. We then calculated the ratio of positive cells in each subset in the stroma for each TMA core. Patient case values were obtained by calculating the mean value of replicate cores of the same patient. Juxta- and distal-epithelial cells were defined based on a threshold distance of 100 Pixels (1 Pixel = 0.3 micrometers) from the epithelial mask.

Statistical analysis

We used a 2-sided Fisher exact association test between 2 categorical variables in cross tabulations. For the analyses of associations between 2 or more categorical variables, the χ^2 test was applied. Mann-Whitney U test was used to test differences between 2 nonnormally distributed continuous variables.

Normality of data was tested using Kolmogorov-Smirnov test. Correlations for continuous variables were calculated using 2-tailed Spearman ρ or Pearson correlation coefficient function. *P* values were calculated using 2-tailed Student *t* test. Differences in juxta- and distal-epithelial compartments were tested using Welch unequal variances *t* test.

For survival analyses, we used Cox proportional hazards regression model and Kaplan-Meier plots with Wald test and log-rank, respectively. Proportional hazards assumption was tested for each variable using the Schoenfeld test. If multiple testing was performed, *P* values were controlled for 10% false discovery rate using Benjamini-Hochberg step-up procedure. *P* values less than .05 were considered statistically significant.

All statistical analyses were performed and visualized using IBM SPSS 26 (SPSS Inc, Armonk, NY, USA), R Statistical Software 3.6.2 (Foundation for Statistical Computing, Vienna, Austria), or Python 3.6.8 using SciPy 1.5.4 library. Data were plotted using R, SPSS, JupyterLab with seaborn library, and Excel (Microsoft, Redmond, WA, USA).

Study approval

The analysis of human tissue specimens and corresponding clinicopathological data was approved by the Uppsala Regional ethical review board (2006/325 and 2012/532) and performed in accordance with the Swedish biobank legislation.

Results

Classification of NSCLC CAFs to 15 subsets using the expression of PDGFRA, PDGFRB, FAP, and α SMA

Two NSCLC tumor collections (BOMI2; $n=318$, and BOMI1; $n=318$) (Table 1) were profiled by multiplex staining with the 4 fibroblast markers and with an anticytokeratin cocktail detecting epithelial cells. Stromal cells were classified into 15 different marker-positive combinations (CAF1 to CAF15) as defined by their binarized status regarding all 4 fibroblast markers: PDGFRA, PDGFRB, FAP, and α SMA (Figure 1, A and B; see Methods for details). Patient case-based values, representing fraction of marker-positive cells belonging to each class, were calculated (Figure 1, A and B). In both cohorts, all 15 subsets were detected and showed large interpatient variability.

The CAF1 (PDGFRA-/PDGFRB-/FAP-/ α SMA+) and CAF5 (PDGFRA-/PDGFRB+/FAP-/ α SMA+) subsets were the most frequent subsets in both cohorts, with fraction values ranging between 10.9% and 21.9% (Figure 1, A and B). The rarest subsets in both cohorts were CAF10 and CAF11, with fraction values ranging between 0.8% and 1.4% (Figure 1, A and B).

Specific analyses of juxta-epithelial and distal-epithelial areas (see Methods) demonstrated that all subsets occurred in both areas (Figure 1, C and D; Supplementary Figure 2, available online). Subsets CAF1, CAF4, CAF6, CAF7, and CAF9 were more common in the juxta-epithelial area in both cohorts (Figure 1, C and D; Supplementary Figure 2, available online).

Pair-wise correlation analyses were performed to explore co-regulation of CAF subsets (Figure 1, E and F). Most pairs were weakly or moderately associated with Pearson correlation coefficient between -0.54 and 0.55 (Figure 1, E and F). Patterns of correlations were overall similar in both cohorts. Strong positive correlations ($P < .001$) were detected between subsets differing in their α SMA status (CAF4 vs CAF5, CAF12 vs CAF13, and CAF14 vs CAF15). In contrast, abundance of CAFs with a PDGFRA-/FAP+ phenotype (CAF2, CAF3, CAF6, CAF7) were inversely correlated ($P < .001$) with those exhibiting a PDGFRA+/FAP-phenotype (CAF8, CAF9, CAF12, CAF13) (Figure 1, E and F). In conclusion, 15 different multimarker-defined NSCLC CAF subsets were observed with varying frequencies and spatial enrichment in juxta-epithelial and distal-epithelial areas.

CAF subset associations with prognosis in NSCLC

The CAF composition exhibited large variability between patients (Figure 2, A). To identify clinically relevant CAF subsets, univariate survival analyses based on continuous values were performed on the pooled cohorts (Figure 2, B). CAF7 (PDGFRA-/PDGFRB+/FAP+/ α SMA+) was associated with poor prognosis, whereas CAF12 (PDGFRA+/PDGFRB+/FAP-/ α SMA-) and CAF13 (PDGFRA+/PDGFRB+/FAP-/ α SMA+) with favorable prognosis (Figure 2, B). Higher fraction of single marker-defined PDGFRA+ cell subset was also associated with better prognosis.

As CAF7 and CAF13 showed the statistically most significant survival associations of the 15 CAFs, we focused on these subsets with additional analyses. Although these CAF subsets showed inverse correlation with each other (Pearson: BOMI2, -0.538; $P < .001$; BOMI1, -0.410; $P < .001$), they were not mutually exclusive (Supplementary Figure 3, A and B, available online).

CAF7 and CAF13 were categorized in both cohorts using median and quartile cutoffs and were examined with Kaplan-Meier plots (Supplementary Figure 4, available online). For both CAF subsets, we combined the 3 quartiles with poorest outcome,

Table 1. Clinicopathological characteristics of the 2 NSCLC cohorts^a

Characteristics	BOMI2 cohort	BOMI1 cohort
Patient sample size and median survival time		
No. of patients	318	318
Median survival time (SD), mo ^b	62 (6)	50 (6)
Age at diagnosis		
Mean (SD), y	66.99 (7.56)	65.61 (8.91)
Median (SD), y	67 (7.56)	67 (8.91)
≤ Median, No. (%)	167 (52.5)	173 (54.4)
> Median, No. (%)	151 (47.5)	143 (45)
Missing data, No. (%)	0	2 (0.6)
Sex, No. (%)		
Male	154 (48.4)	173 (54.4)
Female	164 (51.6)	145 (45.6)
WHO performance status, No. (%)		
0	194 (61)	170 (53.5)
1	121 (38.1)	122 (38.4)
2	3 (0.9)	21 (6.6)
3	0	4 (1.3)
4	0	1 (0.3)
Stage according to pTNM classification, No. (%)		
IA	133 (41.8)	79 (24.8)
IB	73 (23)	137 (43.1)
IIA	35 (11)	8 (2.5)
IIB	31 (9.7)	42 (13.2)
IIIA	39 (12.3)	30 (3.8)
IIIB	0	12 (3.8)
IV	7 (2.2)	10 (3.1)
Histology main groups, No. (%)		
Squamous cell carcinoma	93 (29.2)	112 (35.2)
Adenocarcinoma	186 (58.5)	170 (53.5)
Large cell carcinoma	30 (9.4)	32 (10.1)
Adenosquamous carcinoma	6 (1.9)	0
Others/sarcomatoid carcinoma	3 (0.9)	3 (0.9)
Smoking status, No. (%)		
Ever smoker	282 (88.7)	290 (91.2)
Never smoker	36 (11.3)	26 (8.2)
Missing data	0	2 (0.6)

^a Percentages may not add to 100% due to rounding. NSCLC = non-small cell lung cancer; pTNM = pathological tumor-node-metastasis; WHO = World Health Organization.

^b Median survival times were calculated using the Kaplan-Meier method.

as these resulted with more consistent survival stratifications than using median cutoffs (Figure 2, C and D; Supplementary Figure 4, A and B, available online). Kaplan-Meier analyses confirmed in both cohorts the association with poor and good prognosis of CAF7 and CAF13, respectively (Figure 2, C and D). Analyses on potential survival interactions between the 2 markers did not indicate statistically significant interactions (data not shown). The multimarker-defined PDGFRA+ CAF13 subset showed more consistent survival association than PDGFRA+ cells alone (Supplementary Figure 5, A, available online). Example patient cases with high and low fractions of CAF7 and CAF13 are shown in Figure 2, E and F.

To consolidate findings, we performed analyses on replicate TMA spots separately. Replicate TMA cores showed statistically significant correlation for both CAF7 (BOMI1+2: Pearson = .68; $P < .001$; $n=518$) and CAF13 (BOMI1+2: Pearson = .75; $P < .001$; $n=518$). Both CAF7 and CAF13 showed prognostic significance when their relative fractions from individual TMA cores were analyzed using Cox regression survival analysis (Supplementary Figure 5, B, available online).

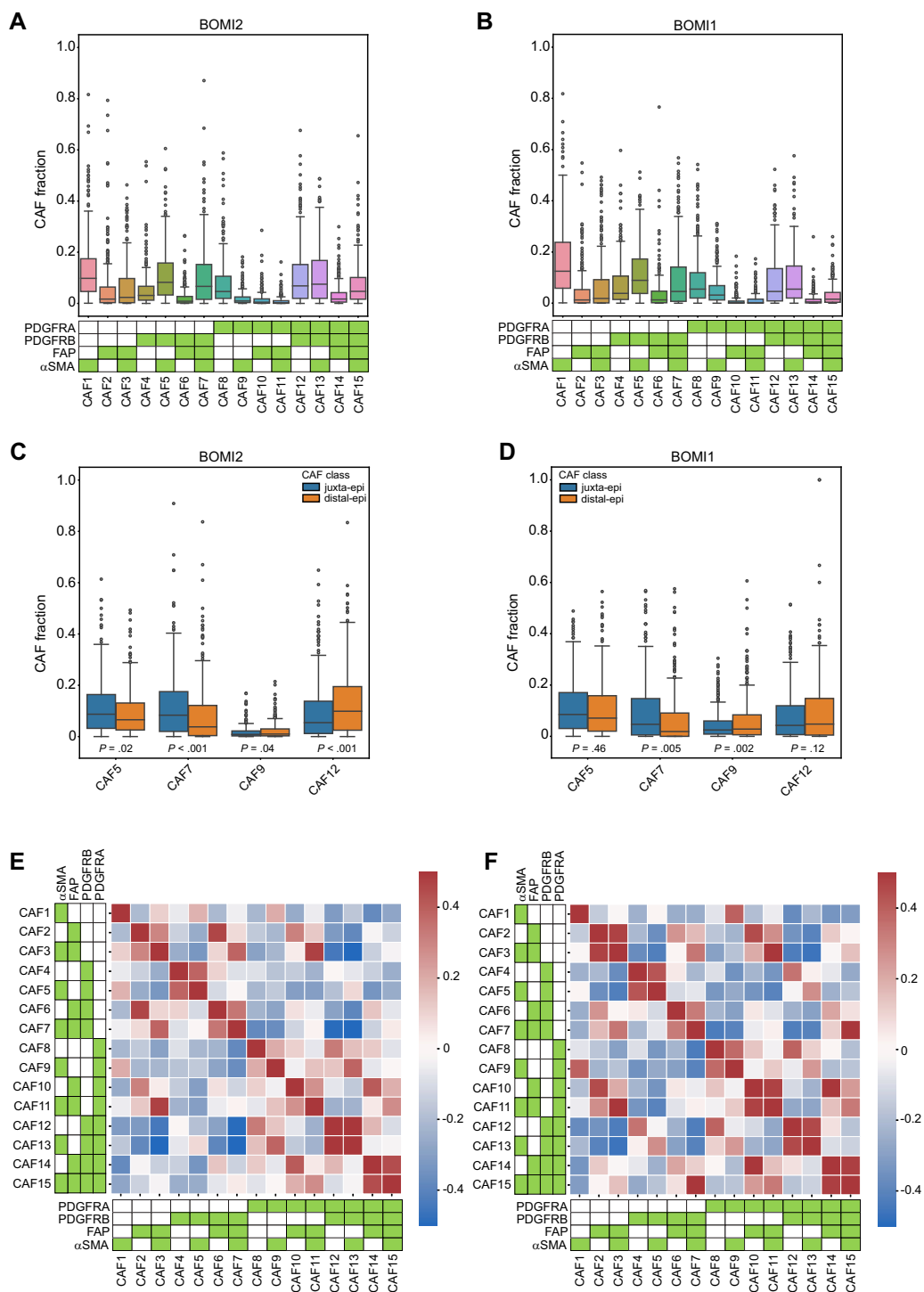


Figure 1. Identification of differentially expressed and spatially enriched multimarker-defined CAF subsets in NSCLC. **A, B** Boxplot representation of relative density of different multimarker-defined CAF subsets in the BOMI2 (**A**) and BOMI1 (**B**) cohorts. **Boxes** represent the interquartile range (IQR) and the **horizontal line** indicates the median. The **whiskers** include values 1.5 times the IQR values. **C, D** Boxplot representation (as in **A, B**) of selected multimarker-defined CAF subsets showing statistically significant differences in relative density in juxta- and distal-epithelial areas of the BOMI2 and BOMI1 cohorts. *P* values with Welch *t* test. **E, F** Heatmap matrix showing patient case-based pairwise Pearson correlation coefficients for relative densities of different multimarker-defined CAF subsets in BOMI2 (**E**) and BOMI1 (**F**). Patients BOMI2, *n* = 318; patients BOMI1, *n* = 318. α SMA = alpha-smooth muscle actin; CAF = cancer-associated fibroblasts; FAP = fibroblast activation protein; NSCLC = non-small cell lung cancer; PDGFRA = platelet-derived growth factor receptor alpha; PDGFRB = platelet-derived growth factor receptor beta.

As the stroma area varies significantly between tumor samples, we also calculated stromal CAF cell density. Both CAF7 and CAF13 remained prognostic with these normalizations ([Supplementary Figure 6](#), available online). When dividing patients into low and high stroma tumors (median cutoff), none

of the CAF subsets were consistently enriched in either group ([Supplementary Tables 2 and 3](#), available online).

Publicly available scRNAseq datasets ([26,36](#)) were examined to compare the FAP+/PDGFRA- CAF7 and FAP-/PDGFRA+ CAF13 subsets with other lung CAF subsets. CAF7 and CAF13 showed

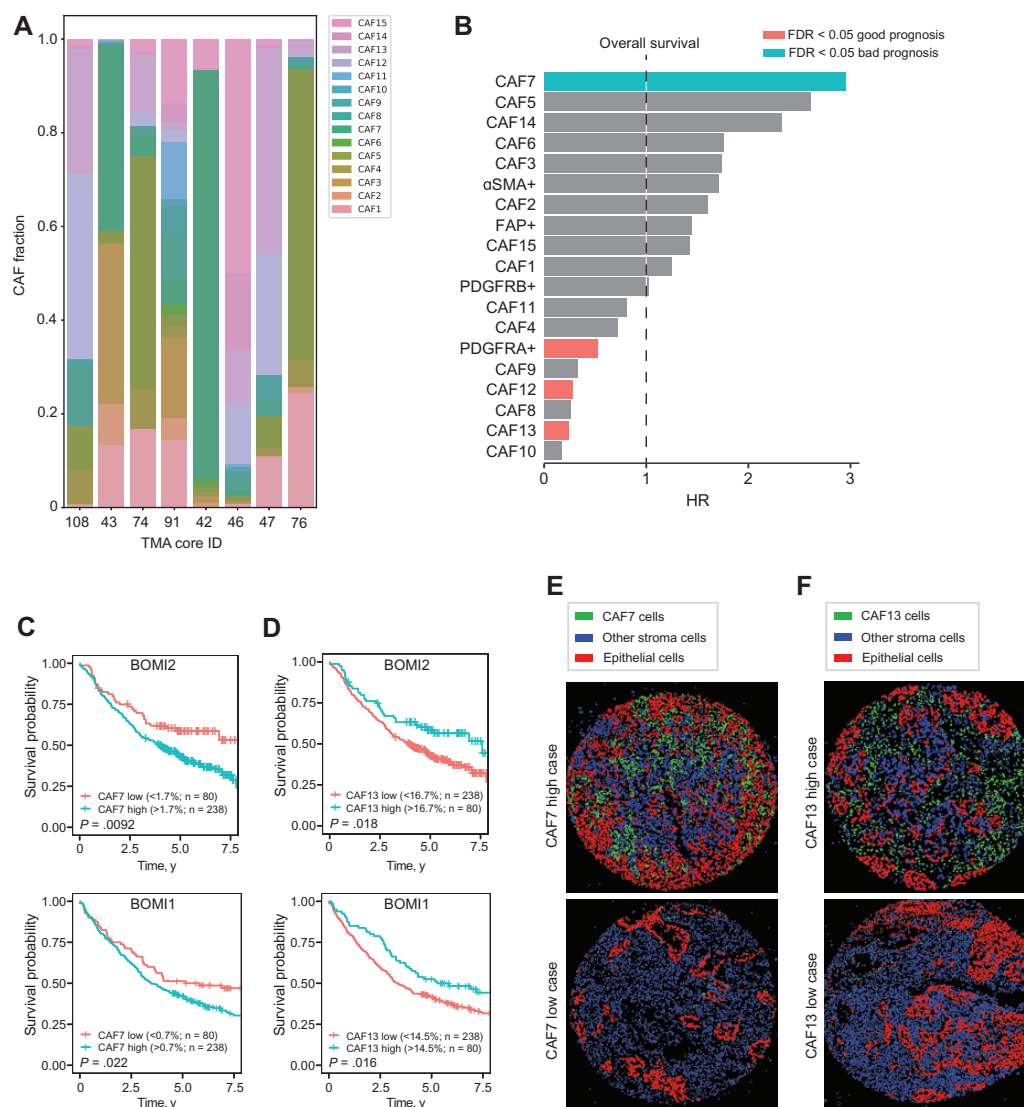


Figure 2. Prognosis associations of NSCLC CAF subsets. **A)** Representation of 15 CAF subsets in 8 selected patient cases highlighting inter-patient variability in their composition. The y-axis fraction represents the percentage from the sum of 15 CAF subsets. **B)** Univariate Cox regression survival analysis of individual CAF markers and multimarker CAF subsets in the BOMI2 and BOMI1 pooled patient cohort ($n = 636$). CAF subsets as single variables (no covariates included) using continuous values. **C, D)** Kaplan-Meier plots of overall survival in the BOMI2 (**upper**) and BOMI1 (**lower**) cohorts according to relative density of FAP+/PDGFRA- CAF7 subset (**C**) and FAP-/PDGFRA+ CAF13 (**D**) subset. FAP+/PDGFRA- CAF7 **red** and **blue** groups correspond to lowest quartile and remainder, respectively; FAP-/PDGFRA+ CAF13 **red** and **blue** groups correspond to the remainder and highest quartiles, respectively. P values from log-rank test. Patients BOMI2, $n = 318$; patients BOMI1, $n = 318$. **E, F)** Pseudocolored cell maps of selected NSCLCs with high (**upper**) or low (**lower**) relative density of the FAP+/PDGFRA- CAF7 (**E**) and FAP-/PDGFRA+ CAF13 (**F**) subsets. α SMA = alpha-smooth muscle actin; CAF = cancer-associated fibroblasts; FAP = fibroblast activation protein; FDR = false discovery rate (multiple measurement adjusted P value); HR = hazard ratio; NSCLC = non-small cell lung cancer; PDGFRA = platelet-derived growth factor receptor alpha; TMA = tissue microarrays.

similarities to previously described CAF clusters 5 and 6, respectively (Supplementary Figure 7, A, available online) in the Lambrechts et al. dataset (26). Furthermore, CAF13 showed similarities to a “COL14A1+ matrix fibroblast subset” in the Kim et al. dataset (36) (Supplementary Figure 7, B, available online).

CAF7 and CAF13 associations with NSCLC histological subtypes

Associations of CAF7 and CAF13 to clinicopathological characteristics were analyzed. CAF7 was significantly enriched in tumors with squamous histology in both cohorts (Table 2). In the BOMI2 cohort, CAF7 and CAF13 were positively and negatively associated with smoking, respectively. CAF7 was significantly associated with higher stage and low performance status in the BOMI2

cohort (Table 2). Neither CAF subsets showed statistically significant associations with age or sex.

CAF7 and CAF13 associations with immune features

Immune profiling data from the BOMI2 cohort was exploited to analyze associations between immune features and the CAF7 and CAF13 subsets. Initial analyses identified most consistent associations of both CAF subsets with programmed death-ligand 1 (PD-L1) expression and density of CD163+ cells (Supplementary Table 4, available online), which were therefore subjected to further analyses.

In the BOMI2 cohort, the CAF7-high patient group showed higher PD-L1 expression (Figure 3, A and B, left) and CD163+ cell

Table 2. Associations of CAF7^a and CAF13^b frequencies with clinicopathological characteristics in BOMI2 and BOMI1 NSCLC cohorts analyzed by contingency tables

Clinicopathological variable	BOMI2 (n = 318)						BOMI1 cohort (n = 318)					
	CAF7			CAF13			CAF7			CAF13		
	Low ^a	High	P ^c	Low	High	P ^c	Low	High	P ^c	Low	High	P ^c
Age at diagnosis, y			.37			2.52			.70			.68
67 and younger	38	129		128	39		42	131		131	42	
Older than 67	41	110		111	40		36	107		106	37	
Missing data	0	0		0	0		1	1		2	0	
Sex			.10			.10			.43			.80
Male	32	122		122	32		46	127		131	42	
Female	47	117		117	47		33	112		108	37	
PS WHO			.006			.22			.48			.15
0	134	60		140	54		42	128		121	49	
1	102	19		96	25		34	88		99	23	
2	3	0		3	0		3	18		16	5	
3	0	0		0	0		0	4		3	1	
4	0	0		0	0		0	1		0	1	
pTNM			.01			.14			.18			.18
IA	47	86		90	43		25	54		51	28	
IB	13	60		57	16		31	106		104	33	
IIA	5	30		28	7		4	4		6	2	
IIB	7	24		24	7		10	32		36	6	
IIIA	5	34		34	5		4	26		24	6	
IIIB	0	0		0	0		4	8		9	3	
IV	2	5		6	1		1	9		9	1	
Histology			<.001			<.001			.007			<.001
Squamous cell carcinoma	9	84		86	7		16	96		98	14	
Adenocarcinoma	62	124		120	66		55	115		110	60	
Large cell carcinoma	6	24		27	3		7	25		27	5	
Adenosquamous	2	4		4	2		0	0		0	0	
Others/sarcomatoid carcinoma	0	3		2	1		1	3		4	0	
Smoking status			.04			.66			.54			.17
Ever smoker	65	217		213	69		70	220		222	68	
Never smoker	14	22		26	10		8	18		16	10	
Missing data	0	0		0	0		1	1		1	1	

^a CAF7 was dichotomized into low and high using the lowest quartile vs remainder. CAF = Cancer-associated fibroblasts; NSCLC = non-small cell lung cancer; PS = performance status; pTNM = pathological tumor-node-metastasis; WHO = World Health Organization grading.

^b CAF13 was dichotomized into high and low using the highest quartile versus remainder.

^c P values were calculated using Fisher exact test.

density (Figure 3, C and D, left). Similar associations were observed regarding immune features in the tumor (Figure 3, A and C) and the stroma compartment (Figure 3, B and D). In contrast, the CAF13-high group exhibited significantly lower PD-L1 expression and CD163+ cell density in tumor and stroma compartments (Figure 3, A-D, left). Histology-specific analyses showed that CAF7 and CAF13 subset associations with PD-L1 expression and CD163 density were observed in the adenocarcinoma group but not in the squamous carcinoma patient group (Figure 3, A-D, middle and right).

In summary, novel associations between immune features and CAF subset composition, particularly prominent in adenocarcinoma, were identified.

CAF7 and CAF13 associations with TP53 and EGFR mutations

Associations between driver mutations and CAF composition were explored using mutation data of the BOMI2 cohort (37). Initial analyses with continuous data for the CAFs suggested associations of both CAF subsets with TP53 and EGFR mutations (Supplementary Table 5, available online).

In the BOMI2 cohort, tumors with high numbers of CAF7 cells were positively and negatively associated with TP53 and EGFR mutations, respectively (Figure 4, A and B). In contrast, tumors with high abundance of CAF13 cells had fewer TP53 mutations

and enrichment of EGFR mutations (Figure 4, A and B). Similar trends were observed in the BOMI1 cohort, where data on mutation status of TP53 and EGFR were available only for 79 of 318 and 165 of 318 patient cases, respectively (Figure 4, C and D).

The mutation comparisons were further conducted in histological subgroups (Supplementary Table 6, available online). In general, trends and statistically significant CAF subset associations with mutations were observed in the adenocarcinoma group, whereas no associations of the CAF subsets with EGFR or TP53 mutations were observed in the squamous cell carcinoma group (Supplementary Table 6, available online).

Taken together, these analyses identified previously unrecognized associations between TP53 and EGFR mutations with specific CAF subsets.

Independence of CAF7 and CAF13 survival associations

Prior findings on the survival associations of CAF7 and CAF13 subsets (Figure 2, C and D) were further developed. Log-rank test of the pooled cohorts confirmed statistically significant poor and good prognosis associations of CAF7 and CAF13, respectively (Figure 5, A and B). The prognostic value of both subsets was particularly strong in low-stage tumors (pathological tumor-node-metastasis [pTNM] IA-IB), PD-L1-negative tumors, and TP53 wild-type tumors (Figure 5, C; Supplementary Figures 8-10, available

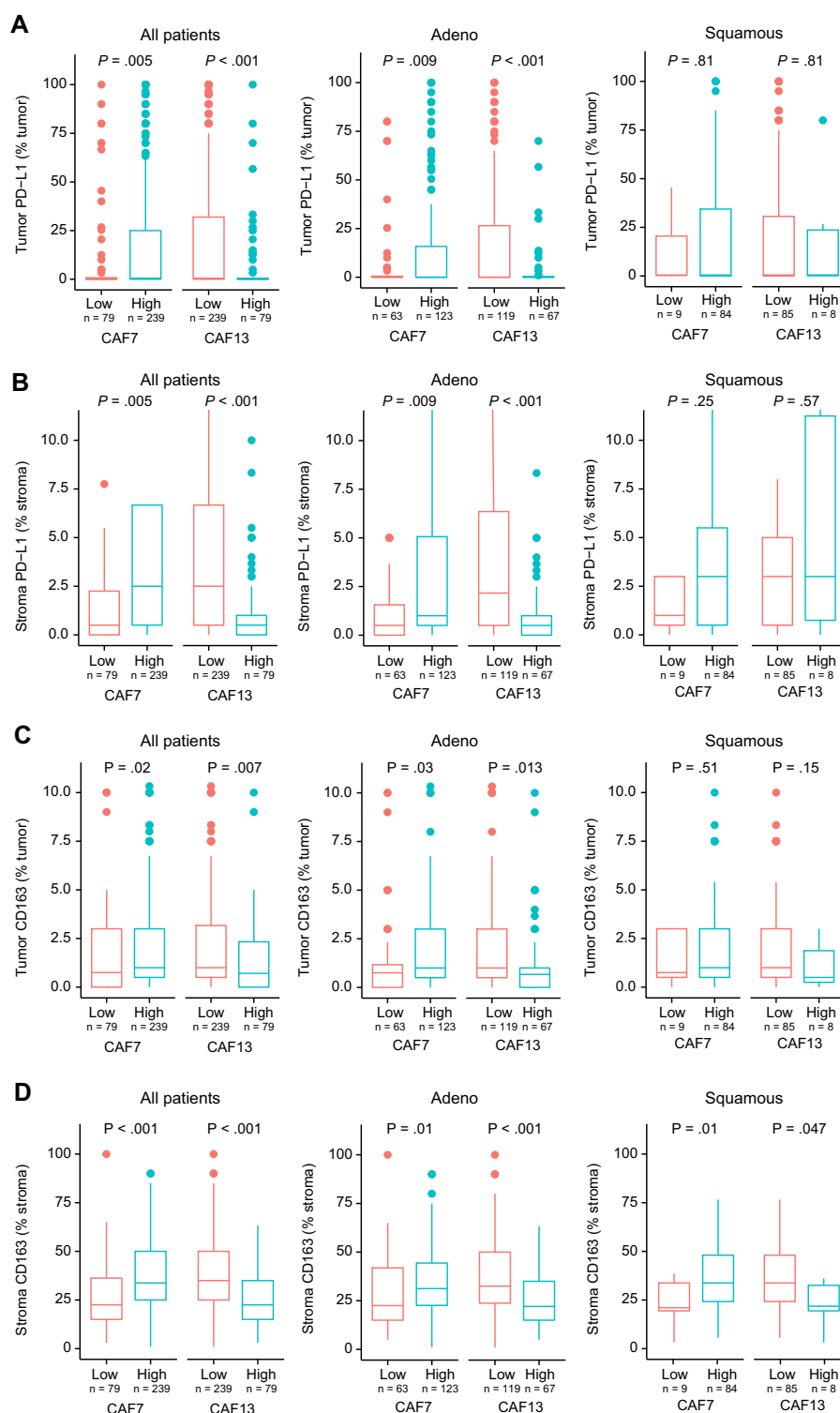


Figure 3. FAP+/PDGFRA- CAF7 and FAP-/PDGFRA+ CAF13 subset associations with immune features. **A)** Expression of PD-L1 in the tumor and **(B)** stroma compartment defined by dichotomized CAF subset status. Dichotomizations were performed as in Figure 2. Expression values represent percentages of positive PD-L1 from the tumor or stroma compartment. **C, D)** Fraction of CD163+ cells in the tumor **(C)** and stroma **(D)** compartment defined by CAF subset status. P values with Mann-Whitney U test. Patients BOMI2, n = 318. Adeno = adenocarcinoma; CAF = cancer-associated fibroblasts; FAP = fibroblast activation protein; PDGFRA = platelet-derived growth factor receptor alpha; PD-L1 = programmed death-ligand 1; squamous = squamous cell carcinoma.

online). Survival analyses were performed separately also on BOMI2 subgroups having received (n = 140) or not having received (n = 150) adjuvant or neo-adjuvant therapy. CAF7 and CAF13 showed similar prognostic trends in the treatment-defined

subgroups as in the full patient cohort (Supplementary Figure 11, available online).

Importantly, CAF7 and CAF13 status independently predicted overall survival in a subgroup of low-stage (pTNM IA-IB) patients

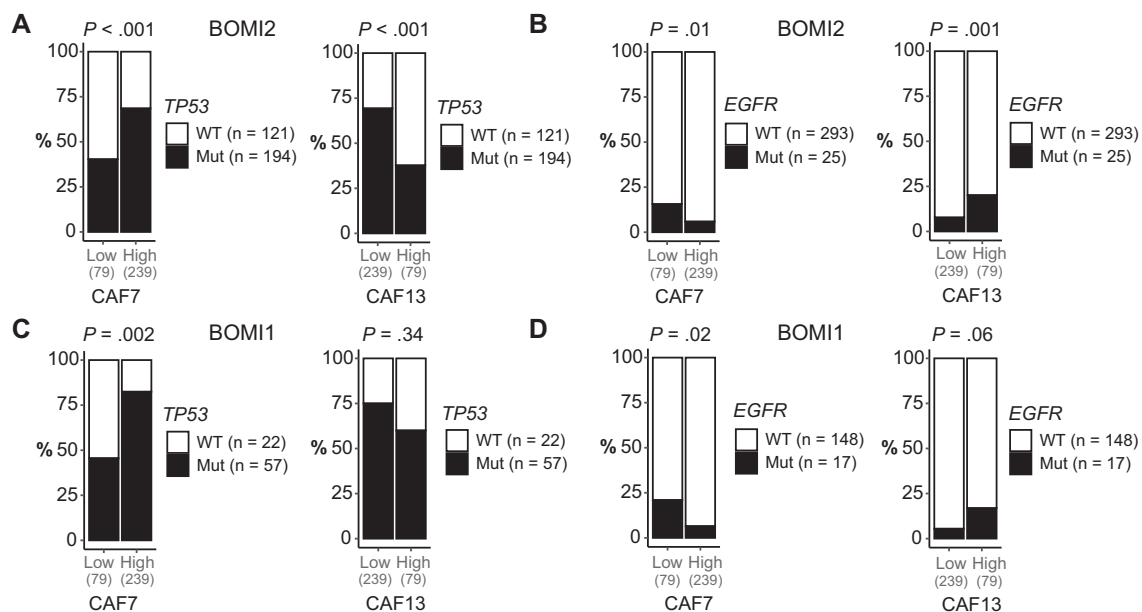


Figure 4. FAP+/PDGFRA- CAF7 and FAP-/PDGFRA+ CAF13 subset associations with TP53 and EGFR mutations. **A, B**) Frequencies of TP53 and EGFR somatic tumor mutations in patients with tumors classified as low or high for CAF7 or CAF13 in the BOMI2 cohort. **C, D**) Same as in **(A, B)** but in patients from BOMI1 cohort. P values with Fisher exact test. Patients with TP53 status in BOMI2, n = 315; patients with EGFR status in BOMI2, n = 315; patients with TP53 status in BOMI1, n = 79; patients with EGFR status in BOMI1, n = 165. CAF = cancer-associated fibroblasts; FAP = fibroblast activation protein; Mut = mutant; PDGFRA = platelet-derived growth factor receptor alpha; WT = wild type.

in a multivariable Cox regression model, also including patient gender, age at diagnosis, and the World Health Organization performance status (Figure 5, D and E).

Validation of CAF7 survival association with external mRNA dataset

Finally, we aimed to validate the prognostic findings using an external dataset. We used bulk mRNA expression data from lung cancer dataset (n = 1925) (38) and performed survival analysis. A high FAP to PDGFRA ratio, partially phenocopying the high CAF7 phenotype (PDGFRA-/PDGFRB+/FAP+/αSMA+), was associated with reduced overall survival (Figure 6, A). When analyzed in a multivariable setting including only low-stage (pTNM IA-IB) patients (n = 574) and adjusted with patient gender and histology, the FAP to PDGFRA gene expression ratio emerged as an independent adverse prognostic factor (P < .001) (Figure 6, B).

Discussion

To the best of our knowledge, this is the most comprehensive study to date on CAFs in a large series of NSCLC. This study identified 2 multimarker-defined CAF subsets with consistent inverse associations with driver mutations, immune features, and outcome, as summarized in Supplementary Figure 12 (available online).

More specifically, the FAP+/PDGFRA- subset (CAF7) exhibited positive associations with squamous histology, immune suppressive features, TP53 mutations, and poor prognosis. In contrast, the FAP-/PDGFRA+ subset (CAF13) exhibited negative associations with squamous histology and immune suppressive features but positive associations with EGFR mutations and good prognosis. With respect to the tumor biology of NSCLC, the most noteworthy findings are the previously unrecognized differential associations between 2 novel CAF subsets and histology, immune features, and driver mutations.

A notable strength of the study is the use of 2 independent well-annotated cohorts with long follow-up. Analyses of the 2 cohorts overall yielded similar results. As a limitation of the study, the absence of mechanistic studies is recognized. The findings suggest a series of novel hypothesis-testing mechanistic studies, as discussed below. Regarding biomarker potential of the CAF subsets, novel studies with well-matched control and treatment groups should be performed to explore treatment-predictive potential of CAF subsets.

A stringent consensus definition of CAFs is still missing. The present study relied on a procedure where marker-positive cells in the stroma were defined as CAFs. Because no negative selection of perivascular areas was performed, it is possible that the 15 subsets include some subsets related to pericytes or vascular smooth muscle cells. However, the marker profile of CAF7 and CAF13 strongly suggests that they represent subsets of true CAF cells.

Previous literature suggests additional markers, such as Thy1 (CD90), FSP1, and integrin beta 1 (CD29), that could be included in future studies. It is possible that that CAF7 and CAF13, as defined in the present study, can be further subdivided based on additional markers.

The associations between immune features and CAF composition provide strong and novel support for the concept of CAFs as important regulators of immune surveillance [reviewed in (4,5)]. The contrasting associations of the 2 CAF subsets with immune-suppressive CD163+ cells might reflect differential effects of the 2 CAF subsets on macrophage polarization and migration, as suggested by earlier studies (20,39-43). Coculture-based functional characterization of FAP+/PDGFRA- CAF7 and FAP-/PDGFRA+ CAF13 cells with macrophages could elucidate their interaction at the cellular level. Notably, the previously described immune suppressive breast cancer S1 subset also exhibited high PDGFRB and FAP expression and may thus be related to the FAP+/PDGFRA- CAF7 subset in the present study (44). Future studies should explore the relationships between the putative immune-

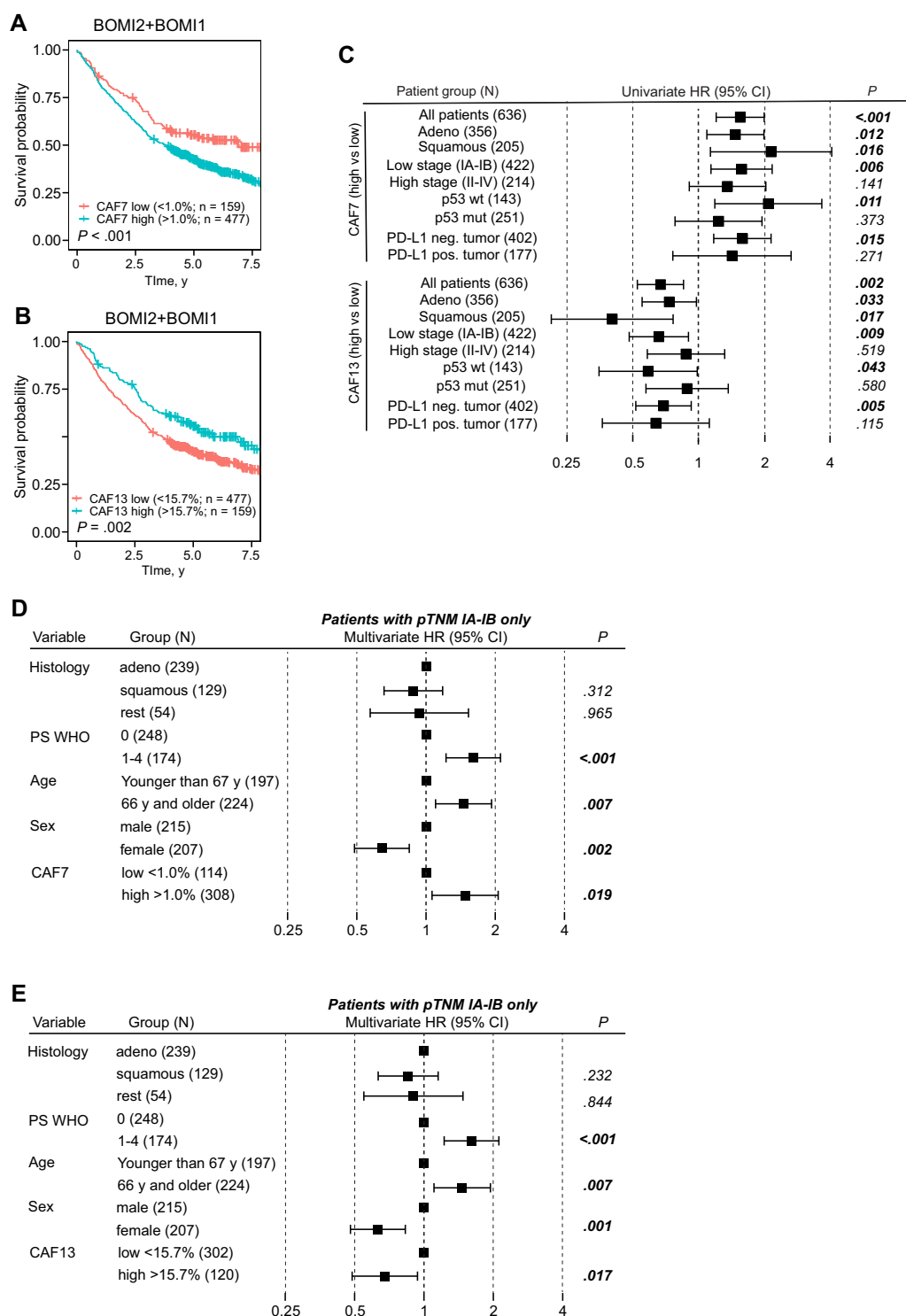


Figure 5. FAP+/PDGFRA- CAF7 and FAP-/PDGFRA+ CAF13 subset associations with survival. **A, B**) Kaplan-Meier plots of overall survival in the pooled BOMI2 and BOMI1 cohorts according to relative density of CAF7 (**A**) and CAF13 (**B**). The CAF7 subgroups correspond to the lowest quartile and the remainder; the CAF13 subgroups correspond to the highest quartile and the remainder. P values from log-rank test (n = 636). **C**) Forest plot of univariate Cox regression survival analysis of CAF7 and CAF13, dichotomized as in (**A, B**) and analyzed separately in the indicated patient subgroups of the pooled NSCLC cohort. **D, E**) Forest plot of a multivariable Cox regression analysis in pTNM IA-IB patient subgroup in the pooled cohort including CAF7 (**D**) or CAF13 (**E**). Adeno = adenocarcinoma; CAF = cancer-associated fibroblasts; CI = confidence interval; FAP = fibroblast activation protein; HR = hazard ratio; mut = mutant; neg = negative; NSCLC = non-small cell lung cancer; PDGFRA = platelet-derived growth factor receptor alpha; PD-L1 = programmed death-ligand 1; pos = positive; PS WHO = performance status based on World Health Organization grades; pTNM = pathological tumor-node-metastasis; squamous = squamous cell carcinoma; wt = wild-type.

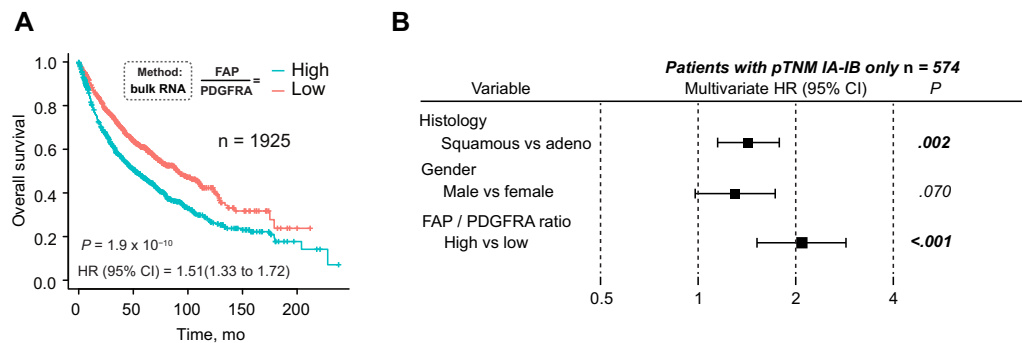


Figure 6. Validation of CAF7 survival association with external mRNA dataset. Bulk mRNA expression data from lung carcinoma [(38)] was analyzed using web interface KM plotter <http://kmplot.com/analysis/>. **A)** Kaplan-Meier plot of OS for FAP/PDGFR α mRNA expression ratio, dichotomized using median cutoff. P value with log-rank statistics; n = 1925 patients. **B)** Forest plot of a multivariable Cox regression analysis in a subgroup of low-stage (pTNM IA-IB) patients; n = 574 patients. Adeno = adenocarcinoma; CAF = cancer-associated fibroblasts; CI = confidence interval; FAP = fibroblast activation protein; HR = hazards ratio; OS = overall survival; PDGFR α = platelet-derived growth factor receptor alpha; pTNM = pathological tumor-node-metastasis.

modulatory CAF subsets described here and other immune-regulatory CAF subsets (13,45,46).

The study suggests that essential driver mutations exert distinct effects on the CAF landscape. It remains unclear if the observed associations between driver mutations and CAF composition reflect effects of driver mutations on recruitment and expansion of CAFs with different cells of origin or effects on the local paracrine microenvironment. Whether TP53 mutations are also associated with the FAP+/PDGFR α -CAF7 phenotype in other tumor types should also be investigated.

From a biomarker perspective, a major new finding of the study is the demonstration that the CAF subsets act as independent prognostic markers. Importantly, no earlier study has reported independent good prognosis survival associations of any CAF subset in NSCLC, despite a series of earlier studies of which some analyzed FAP, PDGFR α , PDGFR β , or α SMA (23-25). Furthermore, the identification of 2 multimarker-defined prognostic CAF subsets elaborates the concept of good CAFs and bad CAFs. One of the defining features of the CAF subsets linked with favorable prognosis is PDGFR α expression. In agreement with the present study, a previous NSCLC study revealed an association with good prognosis of PDGFR α in 1 of 2 analyzed cohorts and an association with good prognosis in the squamous cell carcinoma group of both cohorts (24). In further agreement with the findings of the present study, FAP proportion is associated with poor outcome (25).

The results of this study suggest that the fibroblast subclassification in NSCLC is robust. Notably, results from 2 cohorts stained in different batches and digitized with separate slide scanners were highly concordant. However, optimization of marker cutoffs should be considered for development of CAF-related biomarkers toward clinical practice.

In summary, this study revealed and characterized novel NSCLC CAF subsets with clinical significance. Our findings pave the way for future investigations to better understand the role of CAFs in NSCLC and to utilize them as clinical biomarkers and drug targets.

Funding

This work was supported in part by the Swedish Cancer Society (AÖ, PM), Swedish Research Council (AÖ, PM), the Lions Cancer Foundation Uppsala (PM), and the Sjöberg Foundation (PM), Sweden, the Instrumentarium Science Foundation (TP), the Sigrid

Jusélius Foundation (TP, OK), the Cancer Foundation Finland (OK, 190116; TP, 61-6200), and the Academy of Finland (OK, 333050; LP, 340273 and 337036).

Notes

Role of the funder: The funders had no role in the design of the study; the collection, analysis, and interpretation of the data; the writing of the manuscript; or the decision to submit the manuscript for publication.

Disclosures: The authors declare no competing interests to disclose.

Author contributions: Teijo Pellinen: Conceptualization, Methodology, Validation, Formal analysis, Investigation, Resources, Data Curation, Writing—original draft, Visualization, Supervision, Funding acquisition. Lassi Paavolainen: Software, Formal analysis, Resources, Data curation, Visualization, Writing—Review & Editing. Alfonso Martín-Bernabé: Validation, Formal analysis, Investigation, Resources, Data Curation, Visualization, Writing—Review & Editing. Renata Papatella Araujo: Validation, Formal analysis, Data curation. Carina Strell: Resources, Writing—Review & Editing. Artur Mezheyski: Formal analysis, Resources, Writing—Review & Editing. Max Backman: Formal analysis, Investigation, Resources, Data Curation. Linnea La Fleur: Formal analysis, Investigation, Resources, Data Curation. Oscar Brück: Formal analysis, Resources, Data Curation, Writing—Review & Editing. Jonas Sjölund: Formal analysis, Data Curation, Visualization. Erik Holmberg: Methodology, Formal analysis. Katja Välimäki: Formal analysis, Methodology, Investigation, Data Curation. Hans Brunnström: Investigation, Resources, Data curation. Johan Botling: Investigation, Resources, Data curation. Pablo Moreno-Ruiz: Formal analysis, Investigation, Data Curation. Olli Kallioniemi: Resources, Project administration, Funding acquisition. Patrick Micke: Investigation, Resources, Data Curation, Supervision, Project administration, Funding acquisition, Writing—Review & Editing. Arne Östman: Conceptualization, Resources, Supervision, Project administration, Funding acquisition, Writing—Original Draft.

Acknowledgements: Members of the AÖ group are acknowledged for critical and productive comments during the project. We acknowledge the Institute for Molecular Medicine Finland Digital

Microscopy and Molecular Pathology Unit supported by HiLIFE and Biocenter Finland for scanning services, as well as the Institute for Molecular Medicine Finland High Content Imaging and Analysis unit (HiLIFE, University of Helsinki and Biocenter Finland). We thank Derek Ho, PhD, for language editing.

Data availability

The data underlying this article are available in GitHub, at: <https://github.com/lopaavol/CAF-NSCLC-paper>.

References

- Biffi G, Tuveson DA. Diversity and biology of cancer-associated fibroblasts. *Physiol Rev.* 2021;101(1):147-176.
- Sahai E, Astsaturou I, Cukierman E, et al. A framework for advancing our understanding of cancer-associated fibroblasts. *Nat Rev Cancer.* 2020;20(3):174-186.
- Chen Y, McAndrews KM, Kalluri R. Clinical and therapeutic relevance of cancer-associated fibroblasts. *Nat Rev Clin Oncol.* 2021;18(12):792-804.
- Monteran L, Erez N. The dark side of fibroblasts: cancer-associated fibroblasts as mediators of immunosuppression in the tumor microenvironment. *Front Immunol.* 2019;10:1835.
- Barrett RL, Pure E. Cancer-associated fibroblasts and their influence on tumor immunity and immunotherapy. *Elife.* 2020;9(e57243):1-20.
- Krishnamurthy AT, Turley SJ. Lymph node stromal cells: cartographers of the immune system. *Nat Immunol.* 2020;21(4):369-380.
- McCarthy N, Kraiczy J, Shivdasani RA. Cellular and molecular architecture of the intestinal stem cell niche. *Nat Cell Biol.* 2020;22(9):1033-1041.
- Strell C, Folkvaljon D, Holmberg E, et al. High PDGFRb expression predicts resistance to radiotherapy in DCIS within the SweDCIS randomized trial. *Clin Cancer Res.* 2021;27(12):3469-3477.
- Kawase A, Ishii G, Nagai K, et al. Podoplanin expression by cancer associated fibroblasts predicts poor prognosis of lung adenocarcinoma. *Int J Cancer.* 2008;123(5):1053-1059.
- Paulsson J, Micke P. Prognostic relevance of cancer-associated fibroblasts in human cancer. *Semin Cancer Biol.* 2014;25:61-68.
- Navab R, Strumpf D, Bandarchi B, et al. Prognostic gene-expression signature of carcinoma-associated fibroblasts in non-small cell lung cancer. *Proc Natl Acad Sci USA* 2011;108(17):7160-7165.
- Mezheyeuski A, Segersten U, Leiss LW, et al. Fibroblasts in urothelial bladder cancer define stroma phenotypes that are associated with clinical outcome. *Sci Rep.* 2020;10(1):281.
- Dominguez CX, Muller S, Keerthivasan S, et al. Single-cell RNA sequencing reveals stromal evolution into LRRC15(+) myofibroblasts as a determinant of patient response to cancer immunotherapy. *Cancer Discov.* 2020;10(2):232-253.
- Vennin C, Melenec P, Rouet R, et al.; for the Australian Pancreatic Genome Initiative (APGI). CAF hierarchy driven by pancreatic cancer cell p53-status creates a pro-metastatic and chemoresistant environment via perlecan. *Nat Commun.* 2019;10(1):3637.
- Ostman A. PDGF receptors in tumor stroma: biological effects and associations with prognosis and response to treatment. *Adv Drug Deliv Rev.* 2017;121:117-123.
- Pure E, Blomberg R. Pro-tumorigenic roles of fibroblast activation protein in cancer: back to the basics. *Oncogene.* 2018;37(32):4343-4357.
- Sugimoto H, Mundel TM, Kieran MW, et al. Identification of fibroblast heterogeneity in the tumor microenvironment. *Cancer Biol Ther.* 2006;5(12):1640-1646.
- Lee HW, Park YM, Lee SJ, et al. Alpha-smooth muscle actin (ACTA2) is required for metastatic potential of human lung adenocarcinoma. *Clin Cancer Res.* 2013;19(21):5879-5889.
- Hu H, Piotrowska Z, Hare PJ, et al. Three subtypes of lung cancer fibroblasts define distinct therapeutic paradigms. *Cancer Cell.* 2021;39(11):1531-1547 e10.
- Xiang H, Ramil CP, Hai J, et al. Cancer-associated fibroblasts promote immunosuppression by inducing ROS-generating monocytic MDSCs in lung squamous cell carcinoma. *Cancer Immunol Res.* 2020;8(4):436-450.
- Cruz-Bermudez A, Laza-Briviesca R, Vicente-Blanco RJ, et al. Cancer-associated fibroblasts modify lung cancer metabolism involving ROS and TGF-beta signaling. *Free Radic Biol Med.* 2019;130:163-173.
- Alcaraz J, Carrasco JL, Millares L, et al. Stromal markers of activated tumor associated fibroblasts predict poor survival and are associated with necrosis in non-small cell lung cancer. *Lung Cancer.* 2019;135:151-160.
- Kilvaer TK, Rakae M, Hellevik T, et al. Tissue analyses reveal a potential immune-adjunct function of FAP-1 positive fibroblasts in non-small cell lung cancer. *PLoS One.* 2018;13(2):e0192157.
- Kilvaer TK, Rakae M, Hellevik T, et al. Differential prognostic impact of platelet-derived growth factor receptor expression in NSCLC. *Sci Rep.* 2019;9(1):10163.
- Moreno-Ruiz P, Corvigno S, Te Grootenhuis NC, et al. Stromal FAP is an independent poor prognosis marker in non-small cell lung adenocarcinoma and associated with p53 mutation. *Lung Cancer.* 2021;155:10-19.
- Lambrechts D, Wauters E, Boeckx B, et al. Phenotype molding of stromal cells in the lung tumor microenvironment. *Nat Med.* 2018;24(8):1277-1289.
- Wu F, Fan J, He Y, et al. Single-cell profiling of tumor heterogeneity and the microenvironment in advanced non-small cell lung cancer. *Nat Commun.* 2021;12(1):2540.
- Backman M, La Fleur L, Kurppa P, et al. Infiltration of NK and plasma cells is associated with a distinct immune subset in non-small cell lung cancer. *J Pathol.* 2021;255(3):243-256.
- Edlund K, Madjar K, Mattsson JSM, et al. Prognostic impact of tumor cell programmed death ligand 1 expression and immune cell infiltration in NSCLC. *J Thorac Oncol.* 2019;14(4):628-640.
- Micke P, Mattsson JS, Djureinovic D, et al. The impact of the fourth edition of the WHO classification of lung tumours on histological classification of resected pulmonary NSCCs. *J Thorac Oncol.* 2016;11(6):862-872.
- Micke P, Mattsson JS, Edlund K, et al. Aberrantly activated claudin 6 and 18.2 as potential therapy targets in non-small-cell lung cancer. *Int J Cancer.* 2014;135(9):2206-2214.
- Schindelin J, Arganda-Carreras I, Frise E, et al. Fiji: an open-source platform for biological-image analysis. *Nat Methods.* 2012;9(7):676-682.
- Berg S, Kutra D, Kroeger T, et al. ilastik: interactive machine learning for (bio)image analysis. *Nat Methods.* 2019;16(12):1226-1232.
- Stirling DR, Swain-Bowden MJ, Lucas AM, et al. CellProfiler 4: improvements in speed, utility and usability. *BMC Bioinformatics* 2021;22(1):433.

35. Hollandi R, Szkalitsy A, Toth T, et al. nucleAIzer: a parameter-free deep learning framework for nucleus segmentation using image style transfer. *Cell Syst*. 2020;10(5):453-458 e6.
36. Kim N, Kim HK, Lee K, et al. Single-cell RNA sequencing demonstrates the molecular and cellular reprogramming of metastatic lung adenocarcinoma. *Nat Commun*. 2020;11(1):2285.
37. La Fleur L, Falk-Sorqvist E, Smeds P, et al. Mutation patterns in a population-based non-small cell lung cancer cohort and prognostic impact of concomitant mutations in KRAS and TP53 or STK11. *Lung Cancer*. 2019;130:50-58.
38. Györfly B, Surowiak P, Budczies J, et al. Online survival analysis software to assess the prognostic value of biomarkers using transcriptomic data in non-small-cell lung cancer. *PLoS One*. 2013;8(12):e82241.
39. Kumar V, Donthireddy L, Marvel D, et al. Cancer-associated fibroblasts neutralize the anti-tumor effect of CSF1 receptor blockade by inducing PMN-MDSC infiltration of tumors. *Cancer Cell*. 2017;32(5):654-668 e5.
40. Allaoui R, Bergenfelz C, Mohlin S, et al. Cancer-associated fibroblast-secreted CXCL16 attracts monocytes to promote stroma activation in triple-negative breast cancers. *Nat Commun*. 2016;7(13050):1-20.
41. Yang X, Lin Y, Shi Y, et al. FAP promotes immunosuppression by cancer-associated fibroblasts in the tumor microenvironment via STAT3-CCL2 signaling. *Cancer Res*. 2016;76(14):4124-4135.
42. Lee JW, Stone ML, Porrett PM, et al. Hepatocytes direct the formation of a pro-metastatic niche in the liver. *Nature*. 2019;567(7747):249-252.
43. Davidson S, Efremova M, Riedel A, et al. Single-cell RNA sequencing reveals a dynamic stromal niche that supports tumor growth. *Cell Rep*. 2020;31(7):107628.
44. Costa A, Kieffer Y, Scholer-Dahirel A, et al. Fibroblast heterogeneity and immunosuppressive environment in human breast cancer. *Cancer Cell*. 2018;33(3):463-479 e10.
45. Elyada E, Bolisetty M, Laise P, et al. Cross-species single-cell analysis of pancreatic ductal adenocarcinoma reveals antigen-presenting cancer-associated fibroblasts. *Cancer Discov*. 2019;9(8):1102-1123.
46. Hutton C, Heider F, Blanco-Gomez A, et al. Single-cell analysis defines a pancreatic fibroblast lineage that supports anti-tumor immunity. *Cancer Cell*. 2021;39(9):1227-1244 e20.